

DOI: 10.1070/QEL16051

Efficient gamma-ray generation by ultra-intense laser pulses obliquely incident on a planar plasma layer

D.A. Serebryakov, E.N. Nerush

Abstract. **We have carried out numerical simulations of oblique incidence of a laser pulse with an intensity of $I = 1.33 \times 10^{23}$ W cm^{-2} on a planar plasma layer and found the plasma density and the angle of incidence of p-polarised laser pulses that correspond to the highest gamma-ray generation efficiency and high gamma-ray directivity. The shape of the plasma surface has been determined by simulation and conditions have been considered that lead to an increase in generation efficiency.**

Keywords: *ultra-intense laser pulses, oblique incidence, gamma-ray generation.*

1. Introduction

Since their discovery at the beginning of the 20th century, gamma rays have found application in many areas of science, technology and medicine. At present, the operating principle of most existing gamma-ray sources is based on radioactive decay, bremsstrahlung and inverse Compton scattering, requiring the presence of a radioactive material or the use of large electron accelerators.

A potential alternative approach to gamma-ray generation is to use ultrahigh power laser systems. State-of-the-art femtosecond lasers offer light intensities above 10^{22} W cm^{-2}, and laser systems are being constructed [1] and designed [2] which are expected to allow even more impressive results to be achieved. One of the proposed ways of employing such laser systems is laser wakefield acceleration (LWFA) of electrons using a laser pulse propagating through a plasma and bremsstrahlung gamma-ray generation using the resulting high-energy electron beams [3]. It is worth noting that, at the intensities in question, the dimensionless laser pulse amplitude is $a_0 = eE_0/(mc\omega) \gg 1$ and, driven by the laser field, the electrons begin to efficiently emit photons due to Compton scattering. The photons have a synchrotron spectrum with a characteristic energy of the order of 1 MeV. Previous estimates suggest that, at a sufficiently high laser field intensity, a considerable part of the laser pulse energy can be converted into the energy of gamma-ray photons: several percent for $I \geqslant 10^{22}$ W cm^{-2} [4–6] and tens of percent for $I \geqslant 10^{24}$ W cm^{-2} [7–9]. Because of this, such gamma-ray sources appear very attractive compared to conventional ones and even to LWFA-based sources.

In this paper, we examine gamma-ray generation in the case of oblique incidence of laser pulses on flat targets. Since the ionisation time at the intensities in question is much shorter than the laser wave period, we can consider the interaction of laser pulses with a plasma layer. Section 2 describes the main phenomena that take place in the course of this interaction and lead to efficient gamma-ray generation. In addition, we perform semianalytical modelling of the shape of the plasma surface at oblique incidence of radiation. In Section 3, we present and analyse results of numerical simulation for wide ranges of plasma densities and angles of incidence of laser pulses. We optimise gamma-ray generation parameters and discuss physical effects that ensure the most efficient generation.

2. Interaction process.

We consider a p-polarised pulsed laser radiation incident at an angle θ on a planar supercritical plasma layer. In this configuration, the electric field vector $\boldsymbol{E}$ lies in the plane of incidence and, hence, there is an electric field component E_x normal to the layer (Fig. 1).

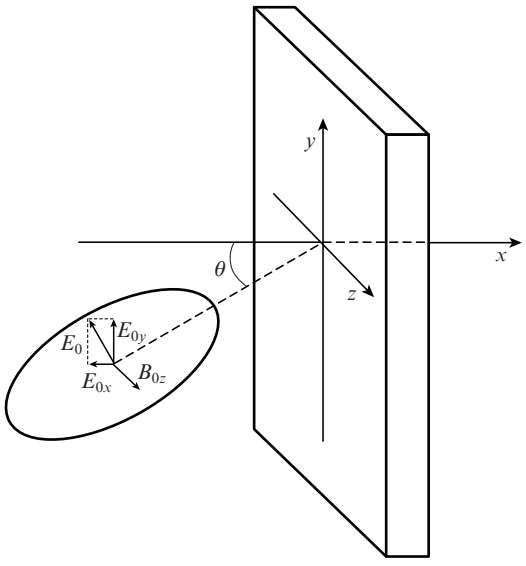

Figure 1. Configuration of the problem of a laser pulse incident at an angle θ on a planar plasma layer.

D.A. Serebryakov, E.N. Nerush Institute of Applied Physics, Russian Academy of Sciences, ul. Ul'yanova 46, 603950 Nizhnii Novgorod, Russia; Lobachevsky State University of Nizhnii Novgorod, prosp. Gagarina 23, 603950 Nizhnii Novgorod, Russia;
e-mail: dms@appl.sci-nnov.ru

Received 24 February 2016
Kvantovaya Elektronika **46** (4) 299–304 (2016)
Translated by O.M. Tsarev

At a plasma density $n_e > \gamma n_{cr}$ [where $n_{cr} = m\omega^2/(4\pi e^2)$ is the critical plasma density at the laser field frequency ω; γ is the characteristic Lorentz factor of electrons interacting with the laser field; and e is the electron charge], the plasma is relativistically opaque to the laser pulse and the pulse penetration depth in the substance does not exceed the thickness of its skin layer. As a rule, $\gamma \sim a_0$ in such processes, so the opacity threshold can be estimated at $n_e = a_0 n_{cr}$.

In the regime under consideration, the ponderomotive force of the laser field shifts electrons to the bulk of the plasma, and they form a thin (compared to the wavelength λ) layer, which to a significant degree screens the external field in the bulk of the plasma (this is suggested by numerical simulation and, moreover, there are models based on this approach [6, 10–12]). Ions have a considerably larger mass, so their motion in the initial stage of interaction (the first few laser field periods) can be neglected. The result is a charge separation field, which can be evaluated to a first approximation using the formula for the field in a planar capacitor: $E_d = \frac{1}{2} e n_e x_d$, where x_d is the displacement of the electron layer relative to its unperturbed position. As the displacement increases, so does the restoring force, and at some instant in time the electron layer begins to move back. The result is an oscillatory process with a period equal to half the laser field period. Because of this, this laser–plasma interaction regime is also referred to as a 'relativistic electron spring' [11]. The above models analytically describe this oscillatory process. Gamma-ray photon emission by electrons in a layer was also modelled previously [12].

It is worth noting one important distinction between the behaviour of electrons at oblique incidence and that at normal incidence. At normal incidence, $E_x = 0$ and the motion of electrons along the x axis is only influenced by the magnetic component of the Lorentz force, which is proportional to $v_y B_z$. At oblique incidence, since there is the component $E_x \neq 0$ and B_z is the same as at normal incidence, the force exerted by the laser field on electrons moving along the x axis increases. This may lead to an increase in the amplitude of electron oscillations in this direction. Numerical simulation indicates that, even at angles of incidence from 5° to 10°, some electrons are plucked out of the plasma (at least in part of their trajectory) and, as the angle of incidence and longitudinal field E_x increase, so does the maximum distance of the electrons from the boundary. This process was analysed by Brunel [13] and Pan et al. [14].

Since the transverse field component (E_y in the case of the polarisation under consideration) is large, as above, such electrons, being essentially in free space, are effectively accelerated by the field along the y axis and acquire high values of the Lorentz factor γ. At external field intensities $I \sim 10^{22}$ to 10^{23} W cm^{-2} and higher, electrons are accelerated to a level $\gamma \sim 100$ and above. The synchrotron emission mechanism then prevails and the emission spectrum lies in the gamma region. Of particular importance is that, according to theoretical calculations and numerical simulation, with increasing I an ever larger part of the laser pulse energy converts to the energy of hard photons. In particular, Ji et al. [8] obtained ~30% efficiency (for $I \sim 10^{24}$ W cm^{-2}) at normal incidence.

It is therefore reasonable to expect that more effective electron acceleration at oblique incidence of laser pulses will lead to an increase in the energy-conversion efficiency from laser radiation to hard photons (relative to the case of normal incidence).

2.1. Modelling of the shape of the plasma surface

At oblique incidence, different points on the boundary plane of a plasma experience the action of the external field with different phases, so the oscillatory process converts into a wave travelling on the plasma surface with a velocity $v = c/\sin\theta$. Using equations of a previously reported model [12], we can determine the shape of the plasma surface. To this end, we transform to a frame of reference moving at a velocity $c\sin\theta$ along the y axis. It can be shown that, in this frame of reference, a laser pulse is incident on the plasma along the normal to its surface [15], but we will have to determine the amplitude and equation of the external field and the plasma density in the moving frame:

$$E' = E\cos\theta, \quad \omega' = \omega\cos\theta, \quad n_e' = n_e/\cos\theta \tag{1}$$

(where the primes refer to the moving frame). Moreover, the equations will include an additional term, describing the field of ions moving at a velocity $c\sin\theta$ in the $-y$ direction.

Modifying equations from Ref. [12] (with no allowance for the reaction force of the light, which has no significant effect on the shape of the plasma surface), we obtain the following system:

$$\begin{aligned} \frac{dp_x}{dt} &= -\frac{n_0 x_d}{2}\left(1 + \frac{v_x v_y^2}{1 - v_x^2}\right) - v_y E_y - \frac{1}{2} v_y n_0 x_d \sin\theta, \\ \frac{dp_y}{dt} &= -\frac{n_0 x_d v_y}{2} - (1 - v_x) E_y + \frac{1}{2}(v_x - 1) n_0 x_d \sin\theta. \end{aligned} \tag{2}$$

All the quantities in Eqns (2) are considered in the moving frame (the primes are omitted). Here $dx_d/dt = v_x = p_x/\gamma$; $v_y = p_y/\gamma$; and $\gamma = \sqrt{1 + p_x^2 + p_y^2}$. In the normalisation used, m, e, $c = 1$; E is normalised to $a_0 = eE_0/(mc\omega)$; n_e is normalised to n_{cr}; and $n_0 = n_e/n_{cr}$.

Integrating these equations, we can find $x_d(t)$ in the moving frame and then return to the laboratory frame. Figure 2 presents the spatial distribution of the electron concentration at a fixed instant of time and numerical simulation results. It is seen that the shape of the plasma surface is rather well described by Eqns (2). More details about the numerical simulation can be found in Section 3.

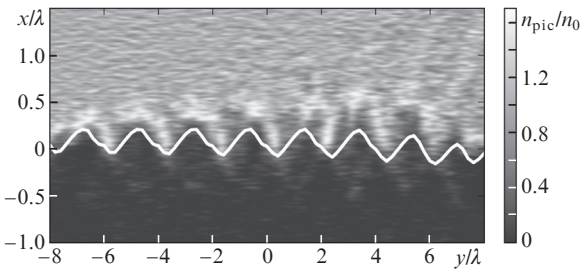

Figure 2. Shape of the plasma surface at $n_0 = 320$ for a laser pulse with $a_0 = 240$ incident at 30° to the x axis. The solid line represents theoretical predictions and the gray-scale pattern represents the electron concentration obtained by PIC simulation.

3. Numerical simulation

We performed several series of numerical simulations of gamma-ray generation as a result of interaction between

obliquely incident laser pulses and a plasma. Three-dimensional simulation was carried out by the particle-in-cell (PIC) method, which has been shown to be effective in simulating laser–plasma interaction processes. The code used allows quantum electrodynamic effects to be taken into account. Emitted hard photons, whose wavelengths are considerably smaller than the mesh size, are modelled as quasi-particles. This is justified at sufficiently high laser field intensities, because a 'synchrotron peak' emerges in the electron emission spectrum at energies corresponding to the synchrotron radiation maximum: $\omega_{\max} = 3c\gamma^3/(2R)$, where R is the radius of curvature of the electron trajectory at a given point. At lower energies, the spectrum has a dip (down to laser harmonics), and waves with wavelengths of the order of the mesh size fall in this zone and are essentially not emitted by the electrons. The applicability of this approach was examined in greater detail by Gonoskov et al. [16]. Photon generation during electron motion along curved trajectories can be simulated by the Monte Carlo method (see the 'alternative' method in Elkina et al. [17]). This allows hard radiation in the region above hundreds of kiloelectron volts to be described with sufficient accuracy.

The longitudinal profile of an incident laser pulse had the form

$$E_{\text{las}}(x) = \frac{\mathrm{d}}{\mathrm{d}x}\left\{\sin x \cos^2\left[\frac{\pi(x + x_{\text{s}})^4}{2x_{\text{s}}^4}\right]\right\}, \tag{3}$$

where the parameter x_{s} determines the pulse duration (in our simulations, it was taken to be $x_{\text{s}} = 5.7\lambda$). The transverse profile had a similar form. The profile has an essentially constant electromagnetic field amplitude in the central part of the pulse and falls off sharply distance x_{s} from the centre. Thus, the problem is brought nearer to an idealised case of incidence of a plane wave on a target and allows the effects resulting from the finite pulse size to be minimised.

The target used was a 2-μm-thick plain film with an ion mass-to-charge ratio four times that of the proton. This roughly corresponds to a heavy element (e.g. Au) target with a degree of ionisation reaching 50% to 70% at the laser pulse intensity and duration under consideration. The laser wavelength was $\lambda = 1$ μm. The mesh size was $(0.1–0.2)\lambda$ and the number of particles per cell was two (test simulations with eight particles per cell revealed no significant differences in results).

3.1. Influence of the angle of incidence and target density on gamma-ray generation efficiency

If the dimensionless laser field amplitude is $a_0 \sim 200$, the electron energy in the course of interaction may reach 100 MeV or more and, in the case of synchrotron emission, most of the energy is emitted in the gamma region. At such high intensities, gamma radiation takes away a considerable part of the incident laser pulse energy (up to tens of percent). Gamma-ray generation efficiency η can be determined as the ratio of the energy of all emitted gamma-ray photons ($\hbar\omega_i$) to the initial laser pulse energy (W_{las}):

$$\eta = \frac{\sum \hbar\omega_i \big|_{t = t_{\text{end}}}}{W_{\text{las}} \big|_{t = 0}} \tag{4}$$

where t_{end} is the end point time of the simulation. Efficiency can be found by numerical calculations using (4) provided that the simulation time is sufficiently long and the size of the simulation region is sufficiently large (the laser pulse should completely interact with the target over time t_{end} and the gamma-ray photons should not have time enough to leave the simulation region).

For a laser pulse with $a_0 = 220$ ($I = 1.33 \times 10^{23}$ W cm^{-2}), we carried out a series of 78 numerical experiments with a variable angle of incidence on the film, 0 to 72°, and different electron concentrations, $(25–150)n_{\text{cr}}$ ($n_{\text{cr}} = 1.11 \times 10^{21}$ cm^{-3} at the parameters used). The laser light intensity and the ranges of angles of incidence and electron concentrations correspond to realistic experimental conditions, where targets from various materials are bombarded in an existing laser system.

Figure 3 shows gamma-ray generation efficiency η as a function of θ and n_0. The maximum value of η is 29%, at $n_0 = 100$ and $\theta = 30°$. The existence of an optimum is an important result, which can be used e.g. in experimental design. The presence of an optimal plasma density can be accounted for as follows: On the one hand, reducing the plasma density leads to a decrease in the number of electrons capable of interacting with the laser field and emitting photons. On the other, with increasing plasma density the penetration depth of laser pulses in the film decreases (at plasma densities above the relativistic self-induced transparency threshold [18], laser pulses are completely reflected from the plasma surface). We also observed a threshold in our numerical experiments. At normal incidence, the n_0 corresponding to the highest gamma-ray generation efficiency was approximately a factor of 2–3 lower than the threshold, $n_0 = a_0$.

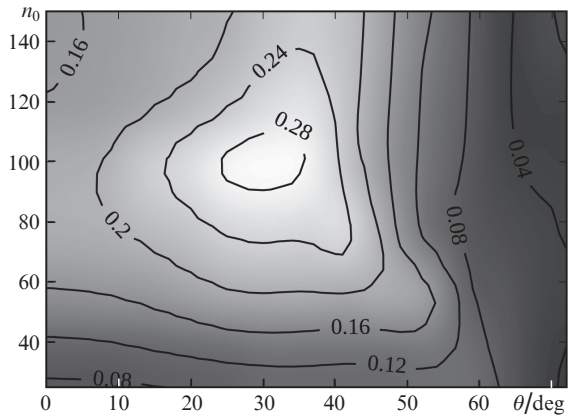

Figure 3. Gamma-ray generation efficiency as a function of plasma density n_0 and angle of incidence θ.

It should be noted that the relativistic self-induced transparency threshold depends on θ. When we transform to a frame of reference moving at a velocity $c\sin\theta$, the external field equation transforms according to (1), whereas the dimensionless amplitude a_0 remains unchanged. The critical plasma density in the new frame has the form

$$n'_{\text{cr}} = n_{\text{cr}}\cos^2\theta. \tag{5}$$

In laser–plasma interaction problems, a similarity law is typically valid [12, 19]: characteristics of interaction (dynamics of particles and radiation parameters) remain similar upon changes in n_{e} and E_y if the n_{e}/a_0 ratio remains unchanged.

Also, a similarity parameter S, which determines interaction conditions, can be introduced as the ratio of the dimensionless plasma density to the dimensionless laser field amplitude:

$$S = \frac{n_0}{a_0} = \frac{n_e}{n_{cr} a_0}. \quad (6)$$

Substituting the transformations from (1), we find that, for S to remain constant, the dimensionless plasma density should vary as follows:

$$n_0(\theta) = n_0(\theta = 0)\cos^3\theta. \quad (7)$$

If the maximum gamma-ray generation efficiency corresponds to a certain value of the parameter S, the position of the maximum $n_{0\max}$ should also be described by (7). In the map presented in Fig. 3, $n_{0\max}$ is seen to have a tendency to decrease roughly as $\cos^3\theta$ as the angle of incidence θ increases from 35° to 60°. At the same time, there is a region in the angular range 25°–40° where $n_{0\max}$ increases with increasing θ. It seems likely that the variation of the characteristics of interaction with θ is inadequately described by the similarity law. This may be due to the presence of additional, angle-dependent terms in the equations [like in (2)].

Figure 4 shows the gamma-ray and electron spectra of the target at the optimal parameters for effective generation (n_0 = 100, θ = 30°). The electron spectrum has a well-defined peak at about 68 MeV. Thus, the typical Lorentz factor (140) is of the same order as a_0 = 220. The highest gamma-ray intensity is observed around 1 MeV, but the intensity decreases rather slowly with frequency, so there is a considerable fraction of gamma-ray photons with energies of tens of megaelectron volts.

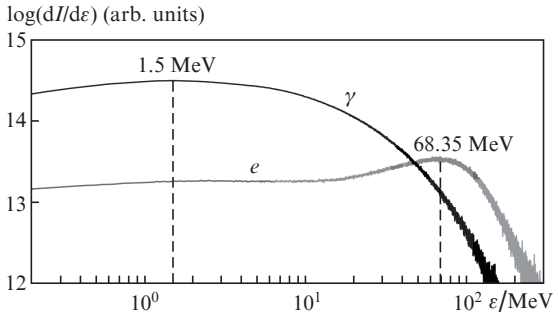

Figure 4. Gamma-ray and electron spectra of the target at n_0 = 100 and θ = 30° (a_0 = 220).

3.2. Radiation pattern of gamma-ray photons

In practical applications, not only high efficiency but also good directivity of gamma-ray generation are important. In contrast to the optical range, gamma rays cannot be focused, so directivity requirements are imposed on sources.

In the case of relativistic laser–plasma interaction, gamma-ray directivity is due to the dynamics of electrons, which emit by the synchrotron mechanism within a narrow cone of angle $1/\gamma$ along their trajectory at each point. The power of the radiation is proportional to the fourth power of the Lorentz factor and the square of the trajectory curvature,

$$I_e = \frac{2e^2 c\gamma^4}{3R^2}, \quad (8)$$

so necessary conditions for efficient and directional emission are that electrons have a large Lorentz factor over an extended part of their trajectory and that the direction of their velocity vector vary only slightly in this part (but the direction should still vary because the radius of curvature of the trajectory should remain not very large). In the case of oblique incidence, this may be facilitated by the fact that electrons enter the $x < 0$ region and the longitudinal field component E_y strongly accelerates them.

Three-dimensional simulation allows one to construct the radiation pattern of gamma rays because the velocity direction and the energy of each photon are known. By analogy with antenna theory, we introduce radiation directivity $\mathcal{D}$ as the ratio of the maximum radiation intensity in the radiation pattern to the intensity averaged over all directions. Thus, $\mathcal{D} = 1$ in the case of an isotropic radiation pattern and $\mathcal{D} \gg 1$ in a highly anisotropic system.

We can also introduce a gain $\mathcal{G}$ as the product of efficiency η and directivity $\mathcal{D}$. $\mathcal{G}$ quantifies the ability of a source to emit intense directional radiation.

Figure 5 shows the $\mathcal{G}$ map for the same values of parameters as in Fig. 3. As above, the distribution has an optimum at an angle θ = 30°, but the corresponding plasma density is lower: n_0 = 75 (against n_0 = 100 in Fig. 3). The most interesting result is the presence of another region with high $\mathcal{G}$, at larger angles ($\theta > 65°$). In spite of the low efficiency, owing to the very high radiation directivity this region is favourable for the generation of relatively intense, directional radiation. Figure 6 illustrates the effect of the angle of incidence on the radiation pattern at n_0 = 100.

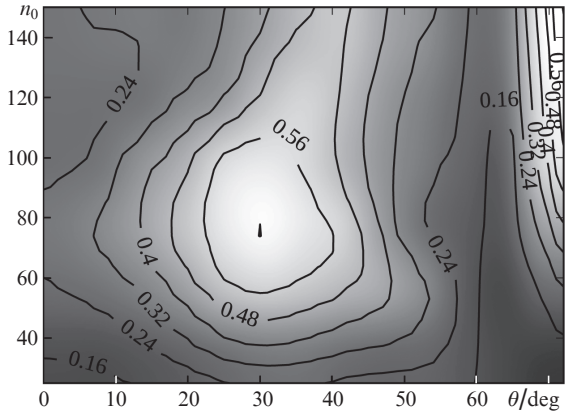

Figure 5. Gain $\mathcal{G}$ as a function of plasma density n_0 and angle of incidence θ.

Our numerical experiments did not cover the angular range $\theta > 72°$ because simulation of a laser pulse incident at a grazing angle to the film requires a substantial increase in the size of the simulation region and computation time and complexity. Nevertheless, we obtained valuable simulation results that allow important effects at large angles of incidence to be highlighted.

The radiation patterns in the xy plane in Fig. 6 help to understand the origin of the second optimal region. There are three distinct types of radiation patterns: two symmetric lobes at $\theta \approx 0$; an asymmetric, but rather broad pattern at intermediate angles of incidence (approximately from 15° to 60°); and a pattern strongly elongated along the y axis for $\theta > 60°$ (in

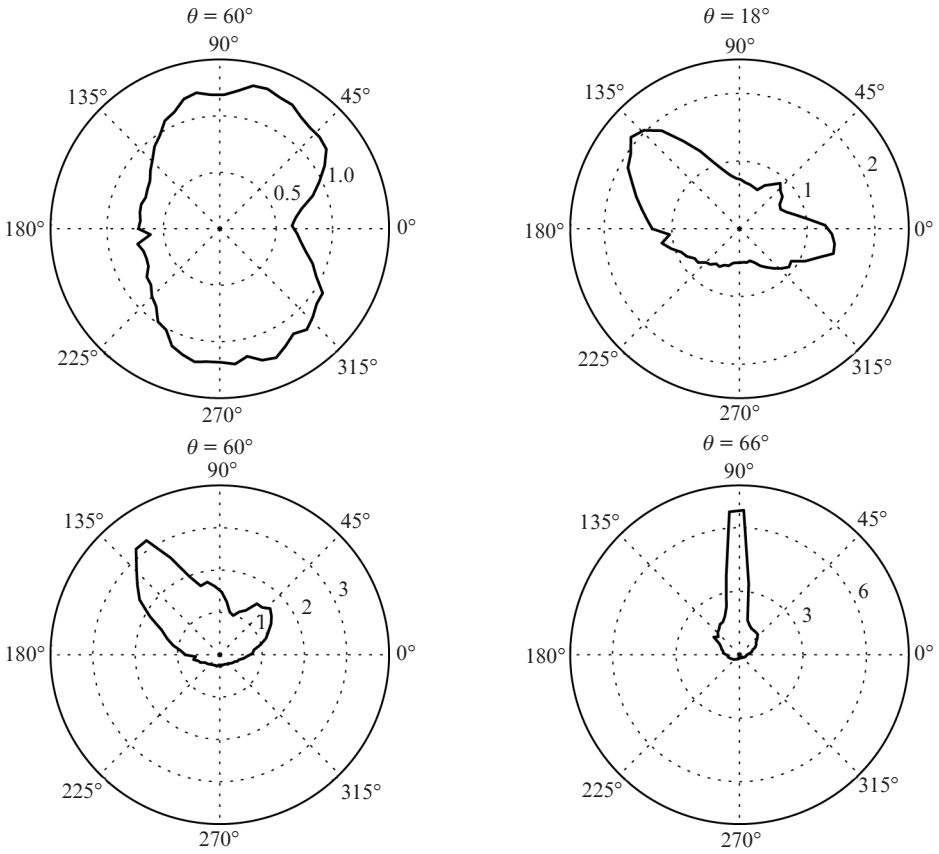

Figure 6. Radiation patterns of gamma rays in the xy plane at $n_0 = 100$ and different angles of incidence θ. The emission angle is measured counterclockwise from the x axis (see Fig. 1).

numerical simulations, it is observed at 66° and 72°). In the last case, the radiation is focused essentially in the propagation direction of the laser pulse.

To understand the cause of the qualitative change in the shape of the radiation pattern for $\theta > 60°$, the characteristics of plasma electrons should be analysed in greater detail using numerical simulation. Figure 7 shows the electron distributions obtained by numerical simulation in x–p_y space at angles of incidence of 60° and 66°. These values of θ were chosen due to the qualitative change in the shape of the radiation pattern (see Fig. 6). Both distributions are obtained at the instants when the trailing edge of the laser pulse reaches the boundary of the plasma. It is seen that, in both cases, electrons with high longitudinal momenta are concentrated mainly near the left boundary of the plasma layer. Moreover, a considerable part of them are located outside the layer ($x < 0$).

An essential distinction is that, at $\theta = 66°$, the number of electrons with very high energies [$p_y/(mc) > 1000$] increases considerably. since the synchrotron radiation intensity is proportional to γ^4, an increase in longitudinal momentum has a very strong effect on the rise in gamma-ray generation efficiency along the y axis, as observed in our numerical experiments.

It is also worth noting that, at $\theta = 66°$, electrons with high p_y are present in the $x < 0$ region somewhat more often than in the $x > 0$ region. This seems to be due to the strong E_x field at large angles of incidence. The increase in the number of electrons outside the plasma layer, in the region of the strong laser field, may be responsible for the increase in radiation intensity at large angles, but further work is needed to identify the exact physical mechanism of this process.

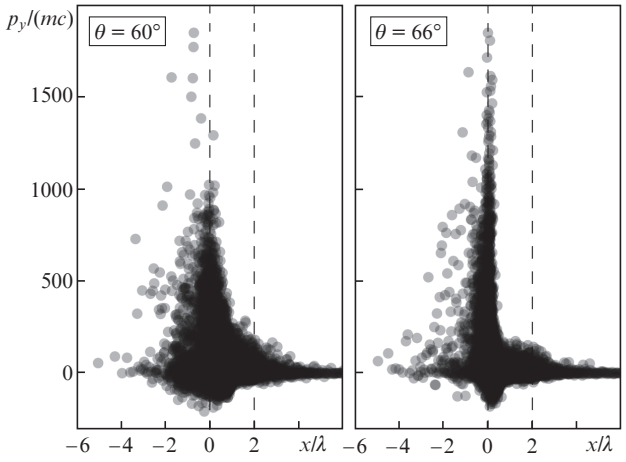

Figure 7. Distributions of the electron momentum component along the layer, $p_y(x)$, obtained by numerical simulation at $n_0 = 100$ and θ = 60° and 66°.

4. Conclusions

At oblique incidence on a flat target with a near-critical relativistic plasma density, relativistic laser pulses with an intensity from 10^{22} to 10^{23} W cm^{-2} are reflected from the film sur-

face, and electrons in the ionised substance are accelerated to relativistic velocities (with $\gamma \sim a_0$). In this process, electrons effectively emit in the hard X-ray and gamma regions. We have carried out three-dimensional simulation of the interaction process and observed efficient conversion of the laser pulse energy to the gamma-ray photon energy with efficiencies up to tens of percent. Optimising the angle of incidence and plasma density, we were able to find efficient generation conditions, which correspond to an angle of 30°. The highest efficiency obtained in numerical experiments at a dimensionless laser field amplitude $a_0 = 220$ is 29%.

Analysis of gamma-ray directivity also demonstrates conditions, at large angles of incidence ($\theta > 70°$), under which radiation is well-focused along the y axis, but the gamma-ray generation efficiency is then not so high. If the purpose is to obtain both an intense and directional radiation source, an optimum is reached in both regimes at $\theta \approx 30°$ and $\theta \sim 70°$. We also have analysed the cause of the qualitative change in the shape of the radiation pattern (radiation localisation along the y axis) at large angles. Numerical simulation indicates a substantial increase in the p_y component of the electron momentum between the $\theta = 60°$ and 66° simulations and an increase in the number of electrons outside the plasma layer. It seems likely that, as a result of the increase in the E_x component of the electric field with increasing θ, electrons are more and more often removed from the plasma and begin to effectively interact with the E_y field. As a result, p_y strongly increases and the emission along the y axis prevails.

We also have carried out a semianalytical modelling of the shape of the plasma surface in the case of interaction with an obliquely incident laser pulse. To this end, we used a modified model for normal incidence [12]. The function thus obtained adequately describes the shape of the plasma surface, which has the form of a wavy structure.

Acknowledgements. This work was supported by the RF Government (Grant No. 14.V25.31.0008) and the Russian Foundation for Basic Research (Grant No. 15-02-06079).

References

1. *Extreme Light Infrastructure.* http://www.eli-laser.eu/.
2. *Exawatt Center for Extreme Light Studies.* http://www.xcels.iapras.ru/.
3. Glinec Y., Faure J., Le Dain L., Darbon S., Hosokai T., Santos J.J., Lefebvre E., Rousseau J.P., Burgy F., Mercier B., Malka V. *Phys. Rev. Lett*., **94**, 025003 (2005).
4. Nakamura T., Koga J.K., Esirkepov T.Zh., Kando M., Korn G., Bulanov S.V. *Phys. Rev. Lett*., **108**, 195001 (2012).
5. Brady C.S., Ridgers C.P., Arber T.D., Bell A.R., Kirk J.G. *Phys. Rev. Lett*., **109**, 245006 (2012).
6. Nerush E.N., Kostyukov I.Yu., Ji L., Pukhov A. *Phys. Plasmas*, **21**, 013109 (2014).
7. Ridgers C.P., Brady C.S., Duclous R., Kirk J.G., Bennett K., Arber T.D., Robinson A.P.L., Bell A.R. *Phys. Rev. Lett*., **108**, 165006 (2012).
8. Ji L.L., Pukhov A., Nerush E.N., Kostyukov I.Yu., Shen B.F., Akli K.U. *Phys. Plasmas*, **21**, 023109 (2014).
9. Brady C.S., Ridgers C.P., Arber T.D., Bell A.R. *Phys. Plasmas*, **21**, 033108 (2014).
10. Rykovanov S.G., Ruhl H., Vehn J.M., Hörlein R., Dromey B., Zepf M., Tsakiris G.D. *New J. Phys*., **13**, 023008 (2011).
11. Gonoskov A.A., Korzhimanov A.V., Kim A.V., Marklund M., Sergeev A.M. *Phys. Rev. E*, **84**, 046403 (2011).
12. Serebryakov D.A., Nerush E.N., Kostyukov I.Yu. *Phys. Plasmas*, **22**, 123119 (2015).
13. Brunel F. *Phys. Rev. Lett*., **59**, 52 (1987).
14. Pan K.Q., Zheng C.Y., Wu D., He X.T. *Phys. Plasmas*, **22**, 083301 (2015).
15. Bourdier A. *Phys. Fluids*, **26**, 1804 (1983).
16. Gonoskov A., Bastrakov S., Efimenko E., Ilderton A., Marklund M., Meyerov I., Muraviev A., Sergeev A., Surmin I., Wallin E. *Phys. Rev. E*, **92**, 023305 (2015).
17. Elkina N.V., Fedotov A.M., Kostyukov I.Yu., Legkov M.V., Narozhny N.B., Nerush E.N., Ruhl H. *Phys. Rev. ST Accel. Beams*, **14**, 054401 (2011).
18. Kaw P., Dawson J. *Phys. Fluids*, **13**, 472 (1970).
19. Gordienko S., Pukhov A. *Phys. Plasmas*, **12**, 043109 (2005).